Journal of Magnetic Resonance 307 (2019) 106580

Contents lists available at ScienceDirect

Journal of Magnetic Resonance

journal homepage: www.elsevier.com/locate/jmr

Static weak magnetic field measurements based on low-field nuclear magnetic resonance

Xiaofei Wang [a,b], Maohua Zhu [a], Kangda Xiao [a,b], Jun Guo [a], Li Wang [a,b,*]

[a] State Key Laboratory of Magnetic Resonance and Atomic and Molecular Physics, National Center for Magnetic Resonance in Wuhan, Wuhan Institute of Physics and Mathematics, Chinese Academy of Sciences - Wuhan National Laboratory for Optoelectronics, Wuhan 430071, China
[b] University of Chinese Academy of Sciences, Beijing 100049, China

ARTICLE INFO

Article history:
Received 23 May 2019
Revised 16 August 2019
Accepted 17 August 2019
Available online 19 August 2019

Keywords:
Low-field NMR
Static magnetic fields
Precession frequency

ABSTRACT

To measure the residual magnetic field, which is a kind of static magnetic fields in the magnetic shields, is a tough task in the design of the cylindrical magnetic shields. Here, we demonstrate a method to measure static weak magnetic fields based on low-field nuclear magnetic resonance (NMR), where the static magnetic field's strength can be obtained by measuring nuclear spin precession's frequency. Atomic magnetometers can be adopted to sense the nuclear spin precession, and the nuclear spin can be adopted to measure the static magnetic field through this indirect method to obtain the static magnetic field's strength. With this method, some adverse factors that can make atomic magnetometers yield fluctuations, such as fluctuations in the light intensity and misalignment of the pump and probe beams, can be avoid. We also measure the axial residual magnetic field in the magnetic shields, where the magnetic field's strength is about 235 pT in the direction along the pump beam. By monitoring NMR signals from protons and fluorine nuclei, we realize a nuclear-spin comagnetometer, which can be used to detect static weak magnetic fields. The possibility of using a miniaturized atomic magnetometer sensor (MAMS) for static field measurements is also discussed.

1. Introduction

High-sensitivity atomic magnetometers have been used to detect weak changing magnetic fields [1–3], such as the magnetic fields that are produced by the brain and heart with physiological and pathological information [4–6], nuclear magnetic resonance (NMR) signals from prepolarized samples [7], and the very weak magnetization from ancient rocks that carry geological information [8]. When designing the magnetic shields, however, precisely measuring residual magnetic fields inside the magnetic shields is difficult. Thus, we demonstrate a method to precisely measure residual magnetic fields based on low-field NMR.

Magnetic-field measurement with NMR was the subject of studies in the mid-1950s, when pickup coils were used to detect nuclear-spin precession [9]. For the proton-precession magnetometer, accuracy of absolute measurement of the Earth's total field is ±10 μG [10]. Although overhauser magnetometers and superconducting quantum interference devices (SQUIDs) have a higher accuracy and higher resolution than the proton-precession magnetometers, they also have disadvantages. The overhauser magnetometer needs a radio frequency to excite the polarization of radical solution in the probe, and it is not easy to shield the radio frequency. The magnetometer relied on SQUID has to be operated at cryogenic temperatures. In recent years, the detection of NMR signals with atomic magnetometers was developed [7]. Based on low-field NMR, we can accurately measure very weak static magnetic fields, such as residual magnetic fields. We can adopt neat liquids or mixed liquids as NMR samples. In this paper, we mainly use protons as the medium for static magnetic field measurements; these proton-rich samples can be held by the NMR sample chamber. The chamber can also load mixtures of miscible solvents, each of which is rich in a different nuclear spin (e.g., a mixture of acetone and hexafluorobenzene). All the protons in acetone have equal weight because acetone is structurally symmetrical. The same is true for the fluorine in hexafluorobenzene. These two species of spins precess at different frequencies because of their different gyromagnetic ratios. These precession frequencies depend on the local static magnetic field; thus, these overlapping ensembles of different spins can be used to measure the static field. We also discuss a type of liquid-state comagnetometer based on these two species of spins in the same volume, as monitored by atomic magnetometer. Unlike atomic magnetometers, which typically employ spins in gas-state systems, comagnetometers that are based on overlapping ensembles of different spins can utilize gas

* Corresponding author.
E-mail address: wangli@wipm.ac.cn (L. Wang).

https://doi.org/10.1016/j.jmr.2019.106580
1090-7807/

states [11] or liquid states [12,13]. As an emerging method, comagnetometers have been used in non-magnetic spin interactions, such as permanent electric dipole moments [14,15], CPT violations [16,17], and spin-gravity coupling [12,13]. Comagnetometers can also be applied to practical applications such as gyroscopes [9,18].

Ledbetter et al. demonstrated a nuclear-spin comagnetometer based on ultralow-field NMR in mixtures of pentane and hexafluorobenzene [12]. Nuclear-spin comagnetometers can be used to measure static magnetic fields through the nuclear spin precession frequency of different species, while atomic magnetometers, rather than inductive rf pickup coil, can be used to detect the precession. Ledbetter et al. showed that the presence of a small magnetic field splits the zero-field J-spectra, imparting plenty of additional information [19]. Wu et al. described a comagnetometer based on the nuclear spins within an ensemble of identical molecules based on zero- to ultralow- field J-coupling [13]. The temperature dependence of J-coupling is considerable, and J-coupling is greatly affected by external factors [20]. In this paper, we present a method research static magnetic field measurements based on non-coupling low-field NMR. The NMR frequencies of non-coupled spins are merely related to magnetic fields, and non-coupled natural abundance samples can also save costs.

The Larmor precession frequency ω of nuclear spins in a magnetic field B is given by [21,22]

$$\omega = \gamma B \tag{1}$$

where γ is the gyromagnetic ratio of the spin and B is the bias magnetic field. Nuclear spins can precess around the bias field; thus, the precession frequency can directly reflect the magnetic field's strength.

Static magnetic field measurements can be used to detect long-term changes of the Earth's magnetic field, the magnetism of ancient rocks and the quantitative magnetic measurement of materials. Such precise magnetic-field measurements can be applied to other fields, such as non-dipole interactions.

2. Theory

Fig. 1 shows a schematic diagram of static magnetic field measurements based on low-field NMR. As an example, the Larmor precession of protons and fluorine nuclei in a mixture of thermally polarized acetone and hexafluorobenzene is monitored with an atomic magnetometer. We apply separate magnetic-field sensors (an atomic magnetometer sensor and NMR sample-chamber sensor) for different types of magnetic field detection. Specifically,

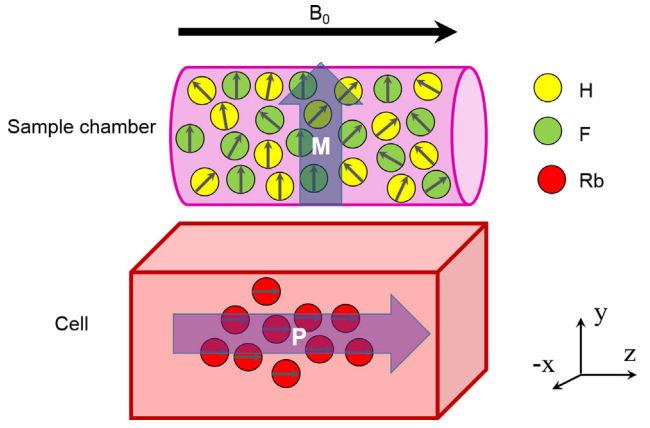

Fig. 1. Schematic diagram of static magnetic field measurements based on low-field NMR. The electron spin polarization $P = 2 < S_z >$ is indicated. **M** is the magnetization vector. $\mathbf{B_0}$ is the bias magnetic field.

the atomic magnetometer sensor detects changing magnetic fields that are produced by the precession of prepolarized nuclear spins, and the NMR sample-chamber sensor detects static magnetic fields, such as the residual magnetic fields in magnetic shields.

In our experimental configuration, we can obtain the response of the atomic magnetometer to quasi-static magnetic fields, producing the components of electronic spin polarization [3,21]:

$$S_x = S_0 \frac{\Delta B B_y + B_x B_z}{\Delta B^2 + (B_x^2 + B_y^2 + B_z^2)} \tag{2}$$

$$S_y = S_0 \frac{-\Delta B B_x + B_y B_z}{\Delta B^2 + (B_x^2 + B_y^2 + B_z^2)} \tag{3}$$

where $\Delta B = (R_{OP} + R_{rel})/g_s\mu_B$, R_{OP} is the pumping rate, R_{rel} is the total spin-relaxation rate, S_i $(i = x, y, z)$ is the electronic spin components, S_0 is the equilibrium electronic spin polarization, and B_i is the magnetic field components.

Because of the magnetic shields, the dominant mechanism of shielding is magnetic flux shunting for static and low-frequency external magnetic fields. At high frequencies, the skin effect plays a dominant role [23]. In this paper, we focus on measuring the residual magnetic field in the shields, where the residual field is close to zero relative to the Earth's field. The atomic magnetometer can directly monitor these dynamic residual magnetic fields. Static residual magnetic fields are difficult to measure because of low sensitivity of the magnetometer in terms of low-frequency fields. However, these fields can be detected based on low-field NMR. In low-field NMR, the spins are polarized in the prepolarization fields, and another low field induces precession in spins that are aligned transversely to the low field. The magnetometer detects dynamic magnetic fields that arise from the precession of nuclear spins. Nuclear spins produce both x and y components of the magnetic field. Specifically, the atomic magnetometer is used to detect NMR signals, which gives the information of the precession frequencies. Although NMR signals have different amplitudes under the same bias fields because of fluctuations in the atomic magnetometer and the polarization time of samples, the precession frequency of NMR signals is the same. The spectral-analysis technique works well for NMR signals of varying amplitude. The magnetic field's strength can be obtained by measuring the precession frequency. For prepolarized samples, the effective field that are experienced by nuclear spins are the positive magnetic field B_+ and the negative magnetic field B_-. These fields act on the samples, which can be expressed as

$$\boldsymbol{B}_+ = (+\boldsymbol{B}_0) + \boldsymbol{B}_R, \quad B_+ = |(+B_0) + B_R| = B_0 + B_R \tag{4}$$

$$\boldsymbol{B}_- = (-\boldsymbol{B}_0) + \boldsymbol{B}_R, \quad B_- = |(-B_0) + B_R| = B_0 - B_R \tag{5}$$

$$\boldsymbol{B}_R = (\boldsymbol{B}_+ + \boldsymbol{B}_-)/2, \quad B_R = (B_+ - B_-)/2 \tag{6}$$

where B_R is the static magnetic field and B_0 is the bias field.

We apply a bias magnetic field $\mathbf{B_0}$ aligned parallel to the z direction, which induces precession in spins. The bias magnetic field should not affect the work of the magnetometer. Therefore, based on the unique design of our magnetic shields, a piercing solenoid is used to provide the bias magnetic field. Solenoids have the characteristics of a uniform internal magnetic field and small-leakage magnetic fields. Solenoid generate magnetic flux that is transported through the magnetic shields, forming a closed loop. Therefore, the external field is a factor of 1000 smaller than the internal field [7,24]. By applying the positive-direction bias field $(+B_0)$ and negative-direction bias field $(-B_0)$ to samples, we can obtain different NMR center frequencies. Internal residual magnetic fields and the magnetic field that is generated by the solenoid are superposed at the position of the samples. Analyzing these NMR signals

enables us to measure NMR-frequency shifts to deduce the corresponding magnetic strength.

Furthermore, we can adopt a mixture of acetone and hexafluorobenzene as the medium to measure the static field, the Larmor precession frequencies of protons and fluorine nuclei of which are

$$\omega_{H+} = \gamma_H B_+, \quad \omega_{H-} = \gamma_H B_- \tag{7}$$

$$\omega_{F+} = \gamma_F B_+, \quad \omega_{F-} = \gamma_F B_- \tag{8}$$

where ω_{H+} and ω_{F+} are the Larmor precession frequencies for protons and fluorine nuclei with a positive magnetic field (B_+), and ω_{H-} and ω_{F-} are those with a negative magnetic field (B_-). In addition, we can set up a nuclear-spin comagnetometer based on an atomic magnetometer. Here, the quotient of gyromagnetic ratios of these two species is a constant, which equates to adding a constraint condition in the static-field measurement. Static magnetic fields can be measured through a difference calculation of the frequencies of nuclei in the mixed solution. If the detected magnetic field changes very slowly over a long period, we still consider the magnetic field to be a static magnetic field and, thus, measurable. The indirect measurement can avoid drift error in long-term measurements and improve the accuracy.

3. Experimental detail

We apply a pump-probe-configuration atomic magnetometer to detect changing magnetic fields. The atomic magnetometer is a vector sensor, the response of which to a small applied field depends on its direction. Hence, we use the magnetometer to monitor the low-field NMR. We can obtain a static magnetic field from these spin-precession frequencies.

The samples are sealed in a special glass chamber that consist of 10-mm NMR tubes. Our sample chambers are completely filled with NMR samples. When the chamber is shuttled between the polarization region and detection region, liquid sloshing is not evident. The temperature of the samples is relatively constant, at about 45 °C. Therefore, we do not consider the atomic spin distribution of the samples from thermal diffusion. The frequency from the spins reflects the *in-situ* magnetic-field strength. In addition, we can move the chamber using nuclear-spin precession to sense the magnetic field from different locations. If the magnetic strength of different sample locations can be measured, we can obtain the magnetic field's gradient.

3.1. Atomic magnetometer

Fig. 2 shows the basic configuration of our experimental setup. The alkali-metal atomic vapor cell works in a high-temperature and ultra-low magnetic-field environment. Our cell is heated to 165 °C to increase the atomic vapor density. We use a set of five-layer cylindrical μ-metal magnetic shields to shield the environmental magnetic field. The amount of conductive materials has to be minimized within the inner magnetic shield to reduce thermal Johnson noise. A set of three-axis magnetic-field coils and three-axis gradient-field coils inside the magnetic shields allows the compensation of the residual magnetic fields. We adopt a two-beam light configuration, where the pump beam is perpendicular to the probe beam in the cell. The pump beam can cause atomic spin polarization, and the probe beam monitors the spin precession from the magnetic fields. Our magnetometer is primarily sensitive to fields in the y direction, with a magnetic field sensitivity of 33 fT/Hz$^{1/2}$ at 32 Hz. This magnetometer also can be operated in several modes to measure different components of the magnetic field [1].

Our magnetometer needs work in low-magnetic-field surroundings. Passive magnetic shields are usually used in weak-precision magnetic-field measurements to create a zero-field region. Therefore, we design two types of magnetic shields: a small set named MS-S and a large set named MS-L. These two sets of shields use the cylindrical magnetic shields as the main components and circular plates as the magnetic shields' cover. For MS-S, the diameter of the inner magnetic shield is 166 mm and the length is 190 mm with a calculated magnetic noise about 17.3 fT/Hz$^{1/2}$. The distance between the laser-beam opening and the sample-transfer passage is 16 mm, and the diameter of the transfer passage is 16 mm. In this paper, the experiment is mainly completed in MS-S. For MS-L, the inner magnetic shield is 300 mm in diameter and 600 mm in length, with a calculated noise of about 6.7 fT/Hz$^{1/2}$. To extend the application of the magnetic shields, we create multiple special rectangular (54 mm × 18 mm) openings. The laser beam, connection wires of coils, samples, etc. can enter the shields through these openings. With these openings, we can study the NMR samples, magnetic fields from rats or other animals, and gradient magnetometers based on the MS-L. We use a flat plate and cylinder as the model to analyze the magnetic noise of magnetic shields from Johnson currents in the μ-metal shields [25]. The magnetometer's detection capability is directly limited by Johnson noise, the effect of which on the magnetometer can be evaluated by using these two shields. The horizontal pneumatic shuttling and MS-S are key components for low-field NMR. We

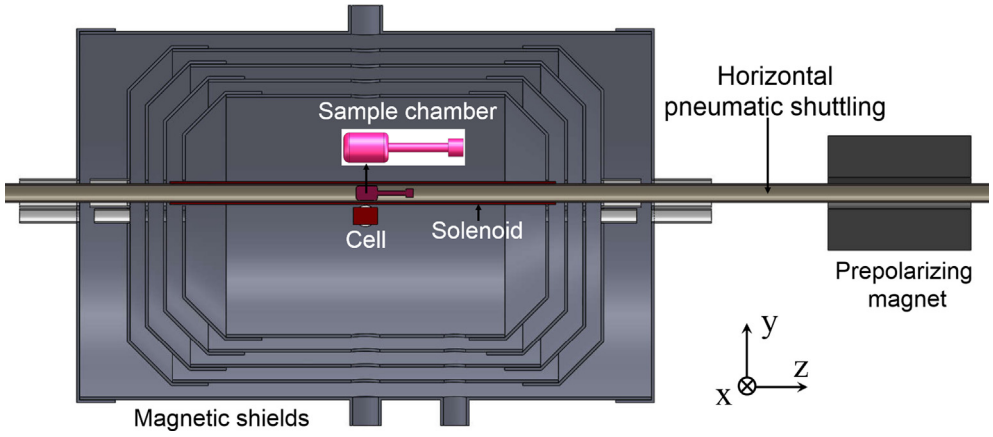

Fig. 2. Experimental setup for low-field NMR based on a rubidium atomic magnetometer, which use the horizontal pneumatic shuttling to transport samples (experimental details described in the text).

realize experimental measurements within MS-S. Moreover, we design MS-L in view of the experimental results from MS-S.

3.2. Low-field NMR

Because of the high gyromagnetic ratio and natural abundance of protons, proton detection is the optimal choice for liquid NMR. We mainly demonstrate proton-based low-field NMR experiments to measure static magnetic fields. The samples are thermally polarized by a 1.5 T prepolarizing permanent magnet. We perform remote detection to avoid magnetizing the magnetic shields, which requires separating the polarization and detection regions. To detect low-field NMR signals, we have to transfer prepolarized samples to the detection region through horizontal pneumatic shuttling. For our configuration, both the prepolarization and precession of sample spins occur in the XY plane, and the magnetometer sensor is sensitive to both B_x and B_y, so DC pulse is unnecessary in the measurements. Then, spin precession is monitored via an alkali-vapor magnetometer. As illustrated in Fig. 3, the time sequence is used for NMR-signal measurements and the corresponding operating state of the horizontal pneumatic shuttling.

A piercing solenoid is used to generate the bias magnetic field that is applied to the NMR samples. The experimental results indicate that the leakage field has a negligible effect on the atomic magnetometer sensor. We create a solenoid with a single-layer copper wire that is wound directly on a quartz-glass tube. The NMR-sample chamber can slide along this quartz-glass tube. Thus, the samples can be shuttled smoothly between the polarization region and detection region. Unlike other pneumatic shuttling devices [7,19,22,26], we demonstrate a new type of shuttling system: a horizontal pneumatic shuttling system. We use this system to transport the NMR samples horizontally, as illustrated in Fig. 3. Axial-magnetic-field measurements are realized through this method. If the chamber sensor is moved away from the magnetometer sensor (fixed), the sample can sense the local static field. The NMR spectrum can be obtained in a single shot, with a 10-s polarization time (or less) and 10–20-s acquisition time. Therefore, this measurement method can provide the distribution of magnetic fields within only tens of seconds and obtain NMR spectra with good frequency resolution.

The simulated static magnetic field is applied to verifying the effectiveness of the static magnetic field measurement method. However, the frequency information from the NMR signals is still subject to chemical shift. Therefore, we have to consider the symmetry of the NMR samples' chemical structures. Acetone and hexafluorobenzene are chosen for their structural symmetry. We demonstrate a comagnetometer based on protons and ^{19}F in a mixture of acetone and hexafluorobenzene. These binary mixtures are rich in different nuclear-spin species, which can support our future research on non-magnetic spin interactions [12].

4. Results and discussion

Fig. 4(a) shows the single-shot raw NMR signal of distilled water, and the inset shows its Fourier transform. To illustrate the utility of low-field NMR, we also examine the case for a mixture of acetone and hexafluorobenzene. Fig. 4(b)–(f) show the single shot low-field NMR signals. To obtain more wave packets, we apply a 738-nT bias magnetic field to induce nuclear precession. These single-shot NMR signals consist of two-frequency signals, which are a superposition of two decaying exponentials, each with their own time constant. These two-frequency NMR signals traveled through a 20–40 Hz band-pass filter. The proton and fluorine produce time-domain NMR signals in both the x and y directions, so the phases of these signals are mixed. From the perspective of differential detection, the NMR frequency information can be simultaneously measured to eliminate some of the error. This error may have originated from gradient magnetic fields and conventional numerical fitting. Gradient magnetic fields shift NMR frequencies and broaden the NMR signals. For conventional numerical fitting, the phase of NMR signals, which is very important for the center frequency of NMR signals that are extracted from the fit, is difficult to determine precisely. However, our data-processing methods are still in development. We prepare mixtures of acetone and hexafluorobenzene with different concentrations (volume ratios of 3:1, 2:1, 1:1, 1:2, and 1:3). The amplitude of each peak proportional to the number of protons and fluorine can be observed by using mixed solutions of different proportions, as shown in Fig. 4(b)–(f). We demonstrate these time-domain signals as fundamental data to verify our measurements and theory. Additionally, the volume ratio of the two mixtures can be deduced by the relative amplitudes of the NMR signals of two nuclei.

The free-precession NMR spectra of protons are shown in Fig. 5. Expanded views of these spectra from 14.6 to 17 Hz are provided. As shown in Fig. 5(a), the static magnetic field measurements are verified by using simulated static magnetic fields. The simulated magnetic fields are calculated from the coil constant, which is also calibrated with a fluxgate magnetometer (magnetic field resolution of 1 nT). The theoretical and measured coil constants (a linear relationship between the magnetic-field strength of the coil and the current) are 90 nT/mA and 89 ± 1 nT/mA, respectively. Here, we consider 90 nT/mA as simulated magnetic-field coil constant. For the low-field (369 nT) NMR of protons, we apply the simulated static fields of 0.72 nT and 1.44 nT and no simulated field to obtain NMR spectra, as shown in Fig. 5(a), and we show the data of any two transients that are obtained without averaging under the same

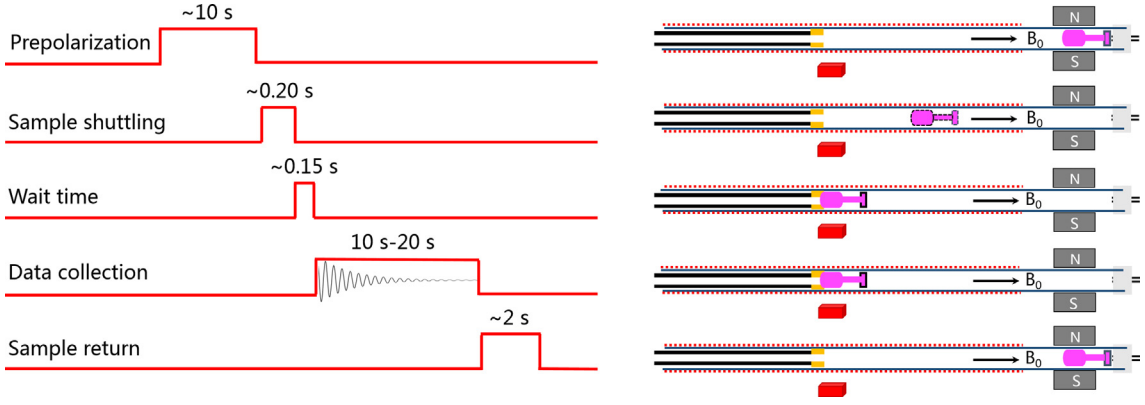

Fig. 3. Time sequence for NMR-signal measurements and the corresponding operating state of the horizontal pneumatic shuttling.

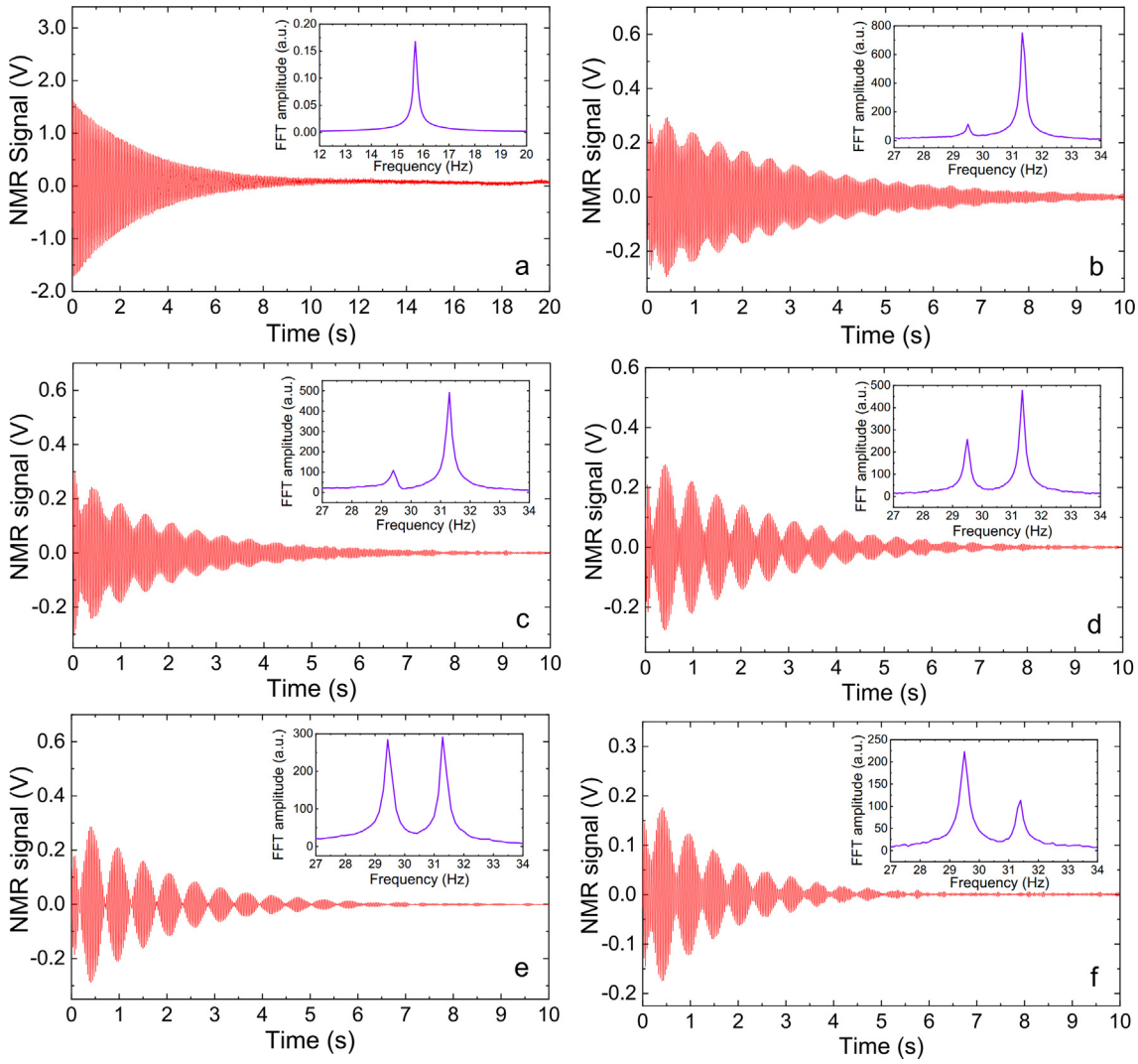

Fig. 4. Low-field NMR signals (single shot). (a) Raw low-field (369 nT) NMR signal obtained in distilled water. Two-frequency low-field (738 nT) NMR filtered signals from a mixture of acetone and hexafluorobenzene with different volume ratios of 3:1 (b), 2:1 (c), 1:1 (d), 1:2 (e), and 1:3 (f). These insets show their Fourier transforms.

simulated field. As shown in Fig. 5(b), we present a set of 0-nT, 0.72-nT, and 1.44-nT spectra with averages that correspond to the traces in Fig. 5(a), where smooth-trace overlaying each data set from the average of these data produce Lorentz profile fitting. Interestingly, these frequency shifts are clearly visible due to differences in the simulated fields. Compared to the case without a simulated static field, the proton's frequency shift of the simulated static field of 0.72 nT is 0.03(05) Hz and that for the simulated field of 1.44 nT is 0.05(91) Hz. These experimental data are in excellent agreement with the theory (γ_H = 42.5775 MHz/T [27]).

The static magnetic field measurement method is used to measure the magnetic field's strength in the axial direction of MS-S. Fig. 5(c) shows the data of three sets under the same experimental conditions based on the low-field NMR of protons. Fig. 5(d) shows the NMR spectra of the positive and negative fields, each resulting from the average of three transients. The experimental data verify a 0.02(42) Hz difference between the positive and negative fields' precession frequencies for low-field NMR. According to Eq. (6), the NMR frequency resulting from the corresponding residual magnetic field is 0.01(21) Hz, which corresponds to a magnetic field strength of 235 (+50) pT. The maximum absolute error is ±0.0015 Hz, which corresponds to a magnetic field strength is ±35 pT. Therefore, we realize the experimental measurements with the MS-S magnetic shield, whose axial-magnetic-field strength is about 235 pT in the z direction (along the pump beam). In the case of magnetic shielding in the geomagnetic field, the shielding factor of the magnetic shielding material is better than 10^5 without considering the magnetism that is carried by the inner magnetic shielding material (the shielding material itself usually has a ∼nT-level field). Our results can be used to evaluate the shielding factor from existing shields and guide the design of new shields for precision measurements. Furthermore, our next step is to develop a more accurate method for directly extracting the frequency from low-field NMR data [28].

This atomic magnetometer that is demonstrated in our laboratory can be applied to research the optimal instrument index and basic physics. The miniaturization of atomic magnetometers is a hot topic in magnetometer design and an important method to expand its applications. A miniaturized atomic magnetometer sensor (MAMS) is an integrated detector with small size, decreasing the detection distance. An MAMS can be utilized to measure the three-axis magnetic fields to reduce the detection distance and improve the signal-to-noise ratio. This miniaturized sensor can be used to detect low-field NMR signals and provide information on the static magnetic field. A three-axis static magnetic field is measured by a MAMS, as illustrated in Fig. 6.

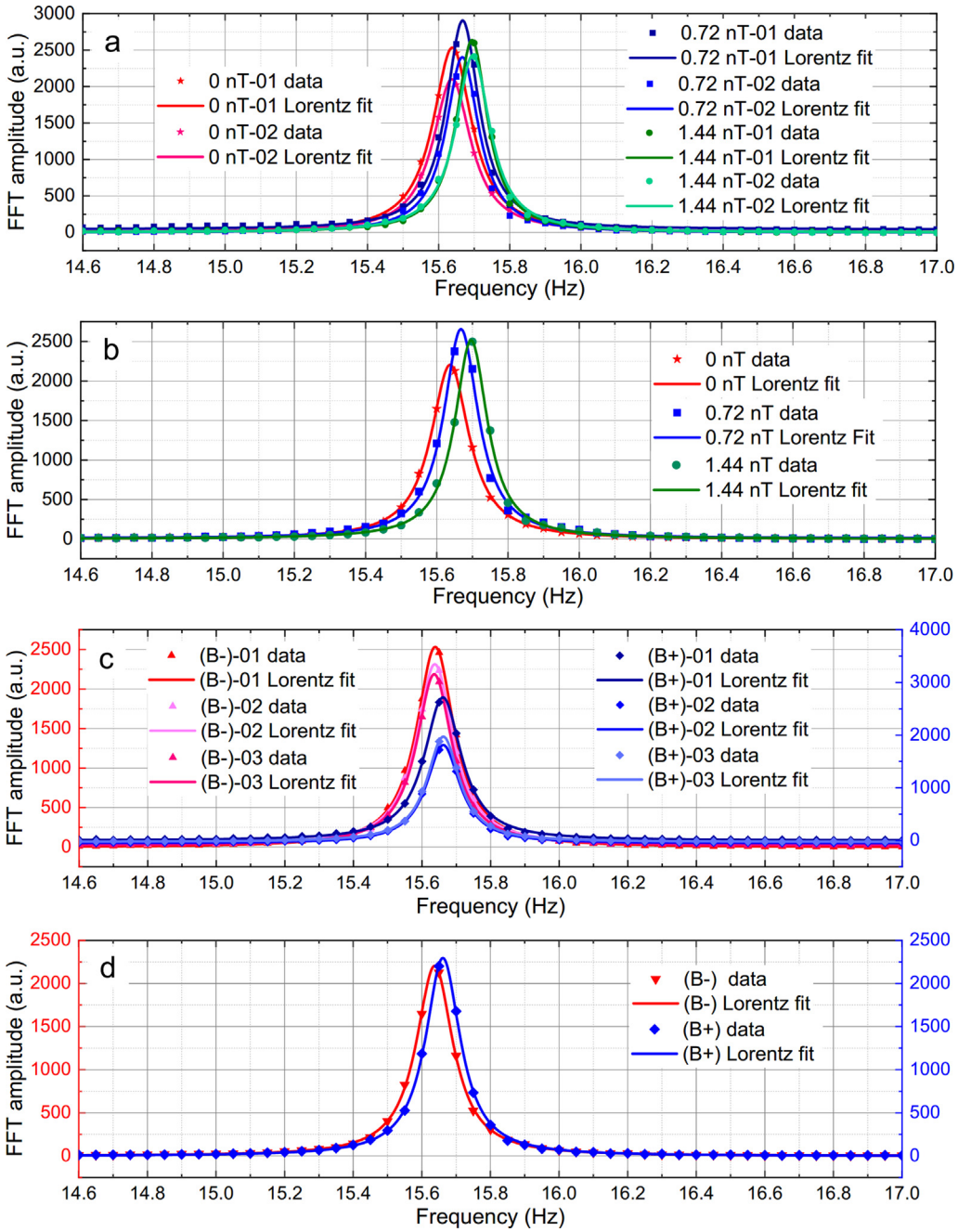

Fig. 5. Experimental demonstration Fourier transforms of low-field NMR signals. (a) Simulated magnetic field measurements and the lines with the best Lorentz fit: the red lines (stars) are obtained with no simulated static field, blue lines (squares) are obtained with a simulated field of amplitude 0.72 nT, and green lines (circles) are obtained with 1.44 nT. (b) Set of 0-nT, 0.72-nT, 1.44-nT spectra, respectively, with averaging and fits. (c) Residual magnetic-field measurements in MS-S: the red lines (triangles) are obtained with the negative-direction bias field (B_{-}) and the blue lines (rhombuses) are obtained with the positive-direction bias field (B_{+}). (d) Smooth traces of NMR spectra with averaging and fits under B_{-} and B_{+}. (For interpretation of the references to colour in this figure legend, the reader is referred to the web version of this article.)

We have used the horizontal pneumatic shuttling for remote detection and realized experimental measurements with MS-S. We design a new magnetic shielding MS-L in view of the experimental results with MS-S. Various methods exist to measure three-axis magnetic fields [29,30], and we propose a new detection method of three-axis static magnetic fields in space. The total field in the three-axis measurement is

$$\boldsymbol{B}_{Total} = \sqrt{\boldsymbol{B}_x^2 + \boldsymbol{B}_y^2 + \boldsymbol{B}_z^2} \tag{9}$$

As shown in Fig. 6, we can move the MAMS and sample chamber along the black arrow to acquire the distribution of magnetic fields. The yellow regions indicate moveable areas, which are the measurement spaces that are limited by the shields openings. Therefore, we present a more rational design of magnetic-shield openings, while cylindrical magnetic shields and their flat covers can use square openings. In the future design of magnetic shields, the dimension parameters must be reasonably configured to effectively expand the application of atomic magnetometers.

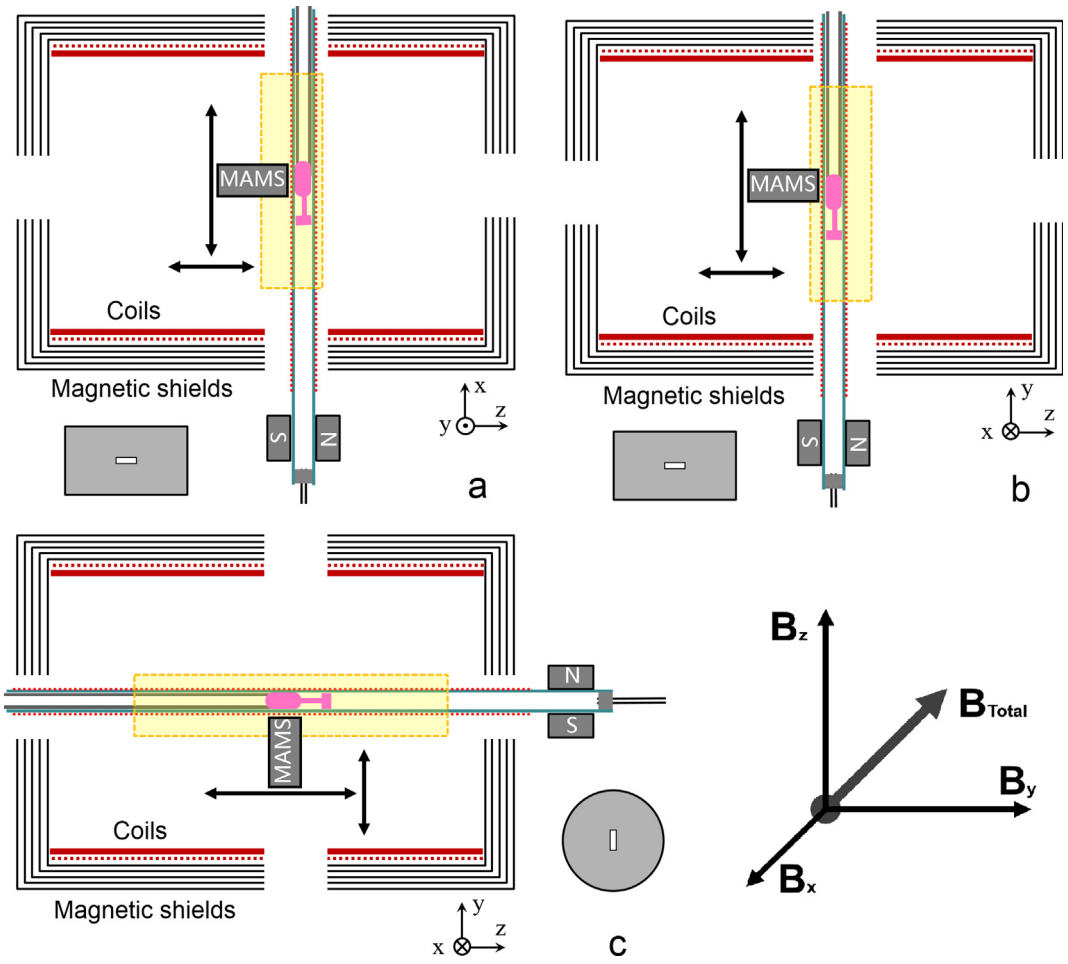

Fig. 6. Schematic of three-axis static weak magnetic field measurements with a MAMS. (a) Magnetic field measurements in the *x* direction, (b) magnetic field measurements in the *y* direction, and (c) magnetic field measurements in the *z* direction.

5. Conclusion

We have demonstrated a new method to measure static weak magnetic fields based on low-field NMR. Analyzing these NMR signals enable us to obtain NMR-frequency information to deduce the corresponding magnetic strength. We show the single-shot raw low-field NMR signals of distilled water and the single-shot filtered signals from a mixture of acetone and hexafluorobenzene under a bias magnetic field as fundamental signals to verify our measurement method. The simulated static magnetic field is applied to confirm the effectiveness of the method. We realize the experimental measurements with the MS-S magnetic shield, whose axial-magnetic-field strength is about 235 pT in the z direction. We also design a new MS-L magnetic shield based on the MS-S experiment. Furthermore, we discuss a nuclear-spin comagnetometer to detect static weak magnetic fields according to NMR signals from protons and fluorine nuclei, which can support our future research on non-magnetic spin interactions. We also propose a theoretical analysis regarding the usage of a MAMS to measure static weak magnetic fields, which is left for a future study.

Acknowledgments

National Natural Science Foundation of China under (Grant No. 11704400); Hubei Provincial Natural Science Foundation of China (Grant No. 2017CFB149). We would like to thank Dr. Shuyi Wei for useful discussions. We would like to thank Xiaoyi Yang, Shuai Nie and Fen Liu for editing the manuscript.

References

[1] J.C. Allred, R.N. Lyman, High-sensitivity atomic magnetometer unaffected by spin-exchange relaxation, Phys. Rev. Lett. 89 (2002) 130801.
[2] I.K. Kominis, T.W. Kornack, J.C. Allred, M.V. Romalis, A subfemtotesla multichannel atomic magnetometer, Nature 422 (2003) 596–599.
[3] M.P. Ledbetter, I.M. Savukov, V.M. Acosta, D. Budker, Spin-exchange-relaxation-free magnetometry with Cs vapor, Phys. Rev. A 77 (2008) 033408.
[4] H. Xia, A.B.-A. Baranga, D. Hoffman, M.V. Romalis, Magnetoencephalography with an atomic magnetometer, Appl. Phys. Lett. 89 (2006) 211104.
[5] D. Budker, M. Romalis, Optical magnetometry, Nat. Phys. 3 (2007) 227–234.
[6] E. Boto, N. Holmes, J. Leggett, G. Roberts, V. Shah, S.S. Meyer, L.D. Muñoz, K.J. Mullinger, T.M. Tierney, S. Bestmann, G.R. Barnes, R. Bowtell, J. Matthew, Brookes, moving magnetoencephalography towards real-world applications with a wearable system, Nature 555 (2018) 657–661.
[7] I.M. Savukov, M.V. Romalis, NMR detection with an atomic magnetometer, Phys. Rev. Lett. 94 (2005) 123001.
[8] H.B. Dang, A.C. Maloof, M.V. Romalis, Ultrahigh sensitivity magnetic field and magnetization measurements with an atomic magnetometer, Appl. Phys. Lett. 97 (2010) 151110.
[9] G.S. Waters, A measurement of the earth's magnetic field by nuclear induction, Nature 176 (1955) 691.
[10] G.S. Waters, P.D. Francis, A nuclear magnetometer, J. Sci. Instrum 35 (1958) 88–93.
[11] T.W. Kornack, R.K. Ghosh, M.V. Romalis, Nuclear spin gyroscope based on an atomic comagnetometer, Phys. Rev. Lett. 95 (2005) 230801.
[12] M.P. Ledbetter, S. Pustelny, D. Budker, M.V. Romalis, J.W. Blanchard, A. Pines, Liquid-state nuclear spin comagnetometers, Phys. Rev. Lett. 108 (2012) 243001.
[13] T. Wu, J.W. Blanchard, D.F. Jackson Kimball, M. Jiang, D. Budker, Nuclear-spin comagnetometer based on a liquid of identical molecules, Phys. Rev. Lett. 121 (2018) 023202.
[14] M.A. Rosenberry, T.E. Chupp, Atomic electric dipole moment measurement using spin exchange pumped masers of ^{129}Xe and ^{3}He, Phys. Rev. Lett. 86 (2001) 22–25.

[15] W.C. Griffith, M.D. Swallows, T.H. Loftus, M.V. Romalis, B.R. Heckel, E.N. Fortson, Improved limit on the permanent electric dipole moment of 199Hg, Phys. Rev. Lett. 102 (2009) 101601.
[16] J.M. Brown, S.J. Smullin, T.W. Kornack, M.V. Romalis, New limit on lorentz- and CPT-violating neutron spin interactions, Phys. Rev. Lett. 105 (2010) 151604.
[17] M. Smiciklas, J.M. Brown, L.W. Cheuk, S.J. Smullin, M.V. Romalis, New test of local lorentz invariance using a ^{21}Ne–Rb–K comagnetometer, Phys. Rev. Lett. 107 (2011) 171604.
[18] E.A. Donley, Nuclear magnetic resonance gyroscopes, IEEE Sensors (2010) 17–22.
[19] M.P. Ledbetter, T. Theis, J.W. Blanchard, H. Ring, P. Ganssle, S. Appelt, B. Blümich, A. Pines, D. Budker, Near-zero-field muclear magnetic resonance, Phys. Rev. Lett. 107 (2011) 107601.
[20] M. Emondts, M.P. Ledbetter, S. Pustelny, T. Theis, B. Patton, J.W. Blanchard, M. C. Butler, D. Budker, A. Pines, Long-lived heteronuclear spin-singlet states in liquids at a zero magnetic field, Phys. Rev. Lett. 112 (2014) 077601.
[21] S.J. Seltzer, Developments in alkali-metal atomic magnetometry, Ph.D. dissertation, Princeton University, 2008.
[22] P.J. Ganssle, Alkali vapor-cell magnetometry and its Application to low-field relaxometry, Ph.D. dissertation, (University OF California, Berkeley, 2014.
[23] D. Budker, W. Gawlik, D.F. Kimball, S.M. Rochester, V.V. Yashchuk, A. Weis, Resonant nonlinear magneto-optical effects in atoms, Rev. Mod. Phys. 74 (2002) 1153–1201.
[24] V.V. Yashchuk, J. Granwehr, D.F. Kimball, S.M. Rochester, A.H. Trabesinger, J.T. Urban, D. Budker, A. Pines, Hyperpolarized xenon nuclear spins detected by optical atomic magnetometry, Phys. Rev. Lett. 93 (2004) 160801.
[25] S.-K. Lee, M.V. Romalis, Calculation of magnetic field noise from high-permeability magnetic shields and conducting objects with simple geometry, J. Appl. Phys. 103 (2008) 084904.
[26] M.C.D. Tayler, T.F. Sjolander, A. Pines, D. Budker, Nuclear magnetic resonance at millitesla fields using a zero-field spectrometer, J. Magn. Reson. 270 (2016) 35–39.
[27] P.J. Mohr, B.N. Taylor, D.B. Newell, CODATA recommended values of the fundamental physical constants, Rev. Mod. Phys. 80 (2008) (2006) 633–730.
[28] A. Wilzewski, S. Afach, J.W. Blanchard, D. Budker, A method for measurement of spin-spin couplings with sub-mHz precision using zero- to ultralow-field nuclear magnetic resonance, J. Magn. Reson. 284 (2017) 66–72.
[29] S.J. Seltzer, M.V. Romalis, Unshielded three-axis vector operation of a spin-exchange-relaxation-free tomic magnetometer, Appl. Phys. Lett. 85 (2004) 4804–4806.
[30] J. Fang, J. Qin, *In situ* triaxial magnetic field compensation for the spin-exchange-relaxation-free atomic magnetometer, Rev. Sci. Instrum. 83 (2012) 103104.